Supplementary Information for

Computational toolbox for ultrastructural quantitative analysis of filament networks in cryo-ET data

Georgi Dimchev [a,1] & Behnam Amiri [b,1], Florian Fäßler [a], Martin Falcke [b], Florian KM Schur [a,*]
[+] *Equal contribution*

Affiliations:
[a] *Institute of Science and Technology (IST) Austria, Am Campus 1, 3400 Klosterneuburg, Austria*
[b] *Max Delbrück Center for Molecular Medicine, Robert Rössle Strasse 10, 13125 Berlin, Germany.*
[1] equal contribution

*** Correspondence to:** florian.schur@ist.ac.at

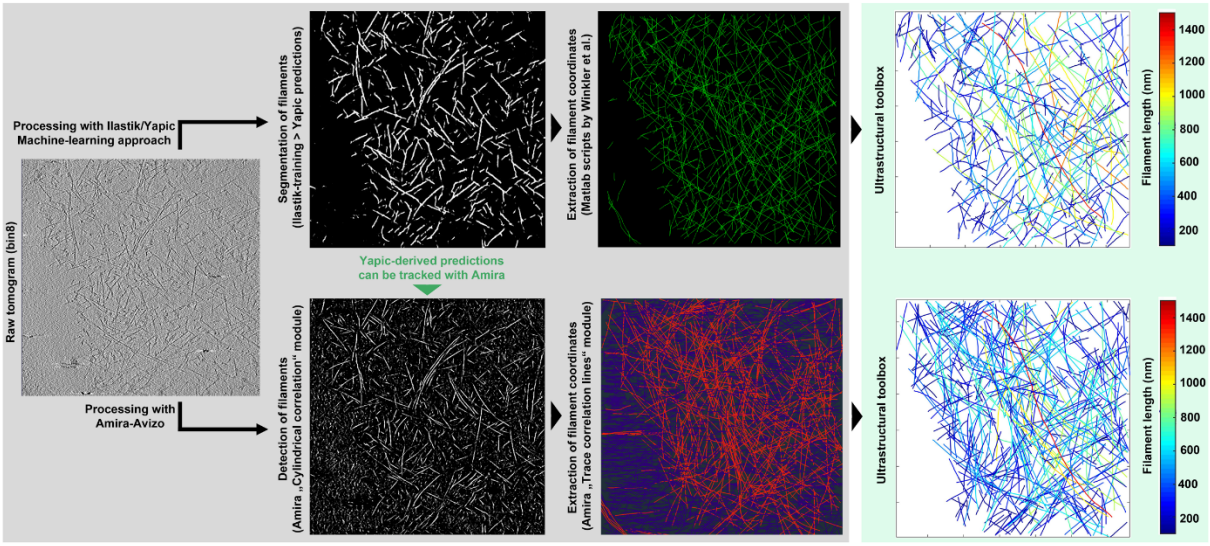

Suppl.Fig-S1. Workflow for extraction of filament coordinate data from cryo-electron tomograms. Here, we compare two alternative, but not mutually exclusive approaches for filament vectorization and extraction of coordinate files. The first approach (upper row, left image) applies the interactive learning and segmentation toolkit Ilastik (Berg et al., 2019), in combination with the YAPiC pixel classifier, to train neuronal networks and generate binary image stacks facilitating the separation of filaments from background. Extraction of filament coordinates data from prediction files (middle panel) can then be performed by available MATLAB scripts (Winkler et al., 2012). An alternative approach (bottom panels) applies the Amira-Avizo software package, where filaments are detected and separated from background via the "Cylindrical correlation" module (left panel) and traced via the "Trace correlation lines" module (middle panel). Notably, the YAPiC-derived prediction files can also be used with Amira-Avizo for downstream segmentation and extraction of filament coordinates information. Right images in both upper and lower panels indicate the visual output extracted from the computational toolbox, color-coded for filament length. The detected filament number/average filament length for both workflows applied to the tomogram in this figure are 297/304. nm with Ilastik/YAPiC (upper panels) and 421/313 nm with Amira (lower panels), respectively. We would like to emphasize that depending on the data type, quality and acquisition settings, any of the two workflows can be fine-tuned to achieve optimal results.

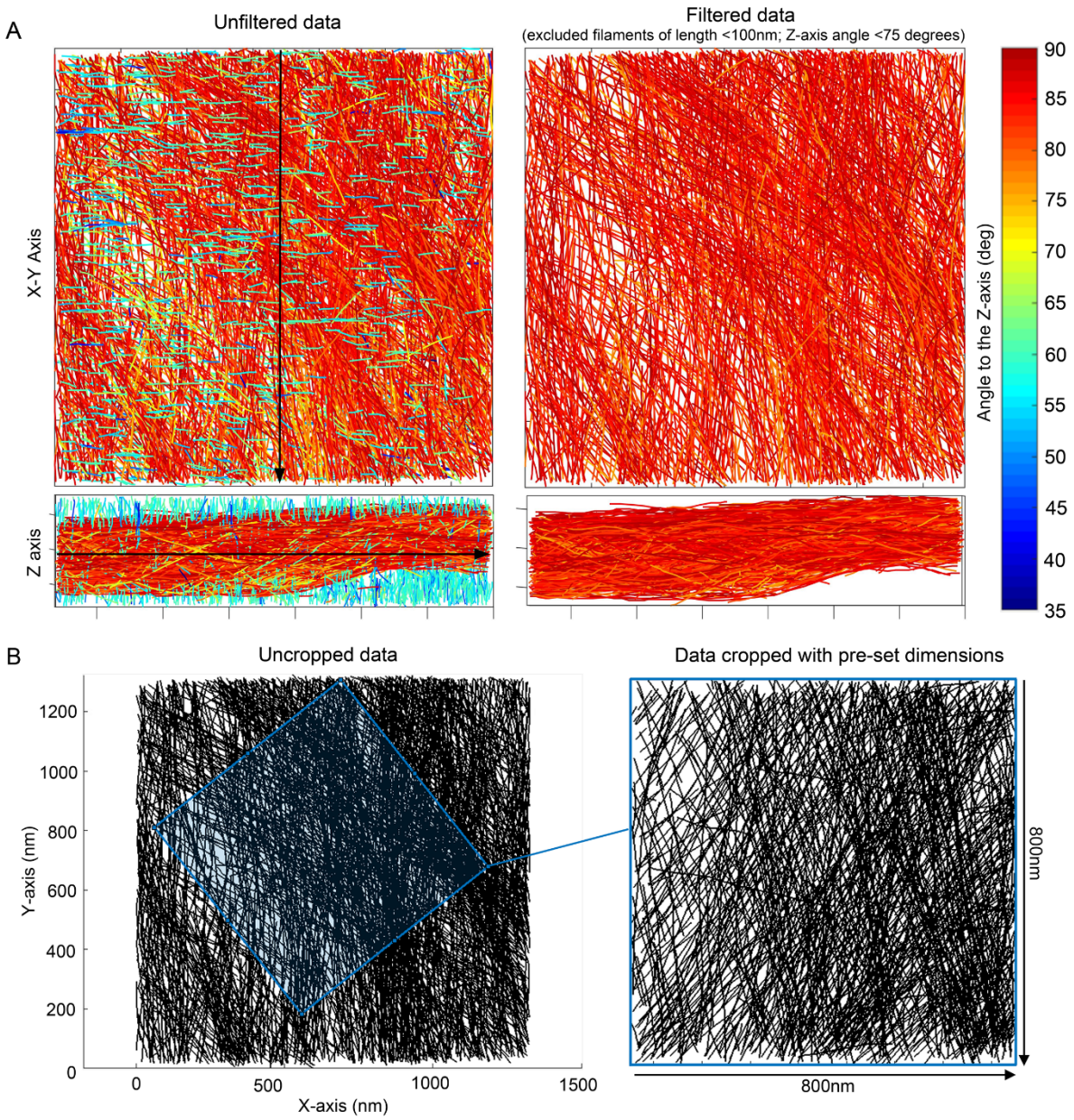

Suppl.Fig-2. Data curation. (A) The toolbox allows removal of unspecific background and to select for analysis only filaments of specific characteristics, via filtering filaments in user-specified ranges for length, bendiness, or angular distribution to X- or Z-axis. The example shows a filamentous network containing unspecific background, manifested as multiple short filaments running approximately perpendicular to the specified X-axis (cyan/green colored filaments in the left panel). The filament network is shown before (left) and after (right) cleaning. The orientation of the X-axis is indicated with a black arrow. **(B)** Datasets containing filament coordinate files of non-uniform dimensions or pixel size can be normalized for downstream analysis by a supplemental cropping script provided with the computational toolbox. An area of desired dimensions can be specified and manually positioned within the coordinate system of each data file (left panel) in order to obtain an output containing only the filament coordinates within the specified dimensions (right panel).

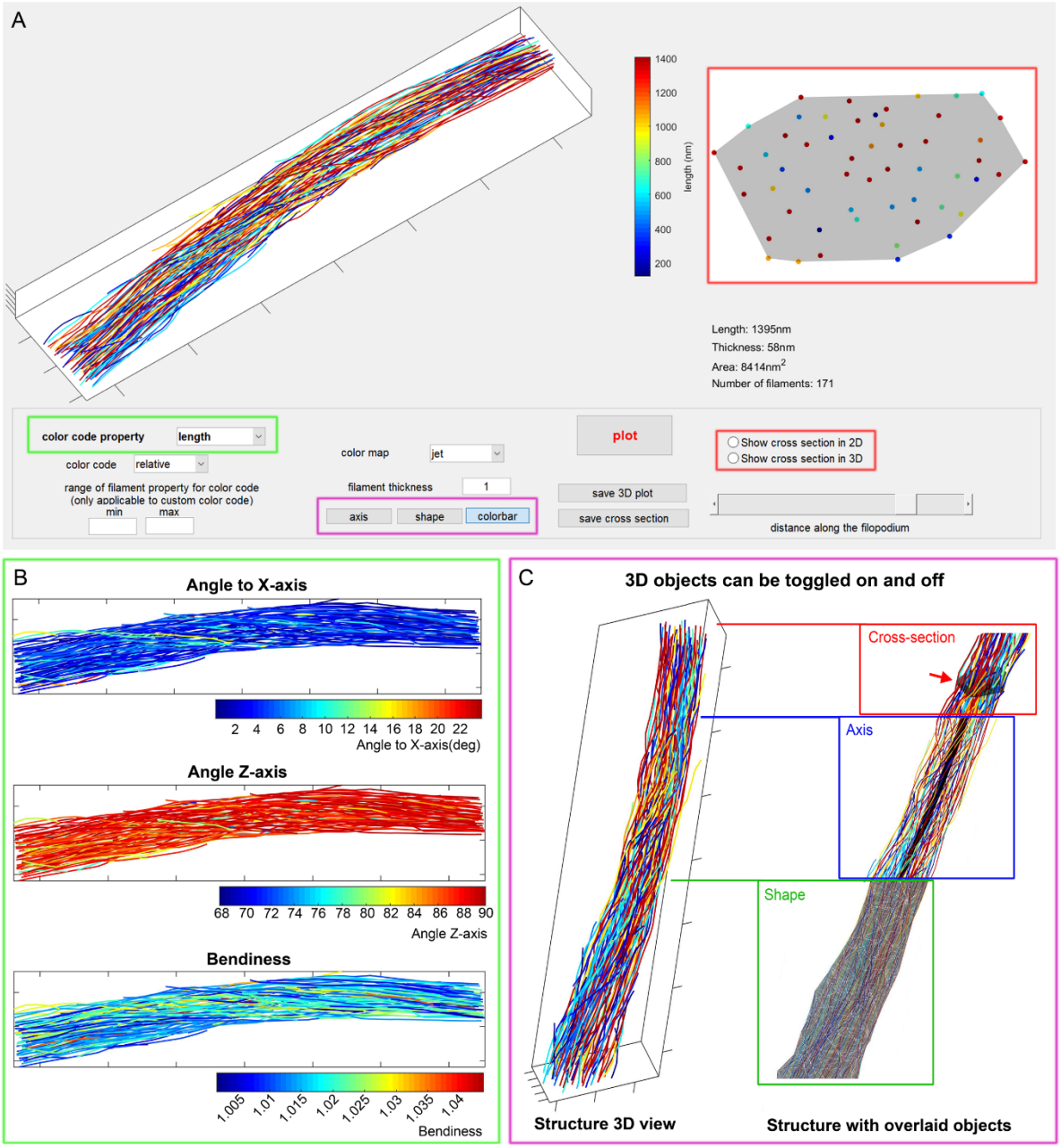

Suppl.Fig-3. Visualization module. (A-C) The GUI-based 3D visualization module integrated in the computational toolbox allows for customized structure visualization. Filament color coding can be based on selectable ranges for length, bendiness, or angular orientation (the green rectangle shows the selected option in panel **(A)** and three alternative output examples shown in panel **(B)**. Objects, such as axis, shape or color bar, can be displayed together with the structure (purple rectangles in **(A)**) with respective examples in **(C)**. The module allows visualizing the cross-sectional orientation of filaments (red rectangles in **(A)**), with the position of the cross-section being adjustable along the axis of the structure (red arrow in (C)). More information on the structure, such as length, thickness, area covered, and the number of filaments contained is also given below the cross-section visualization panel.

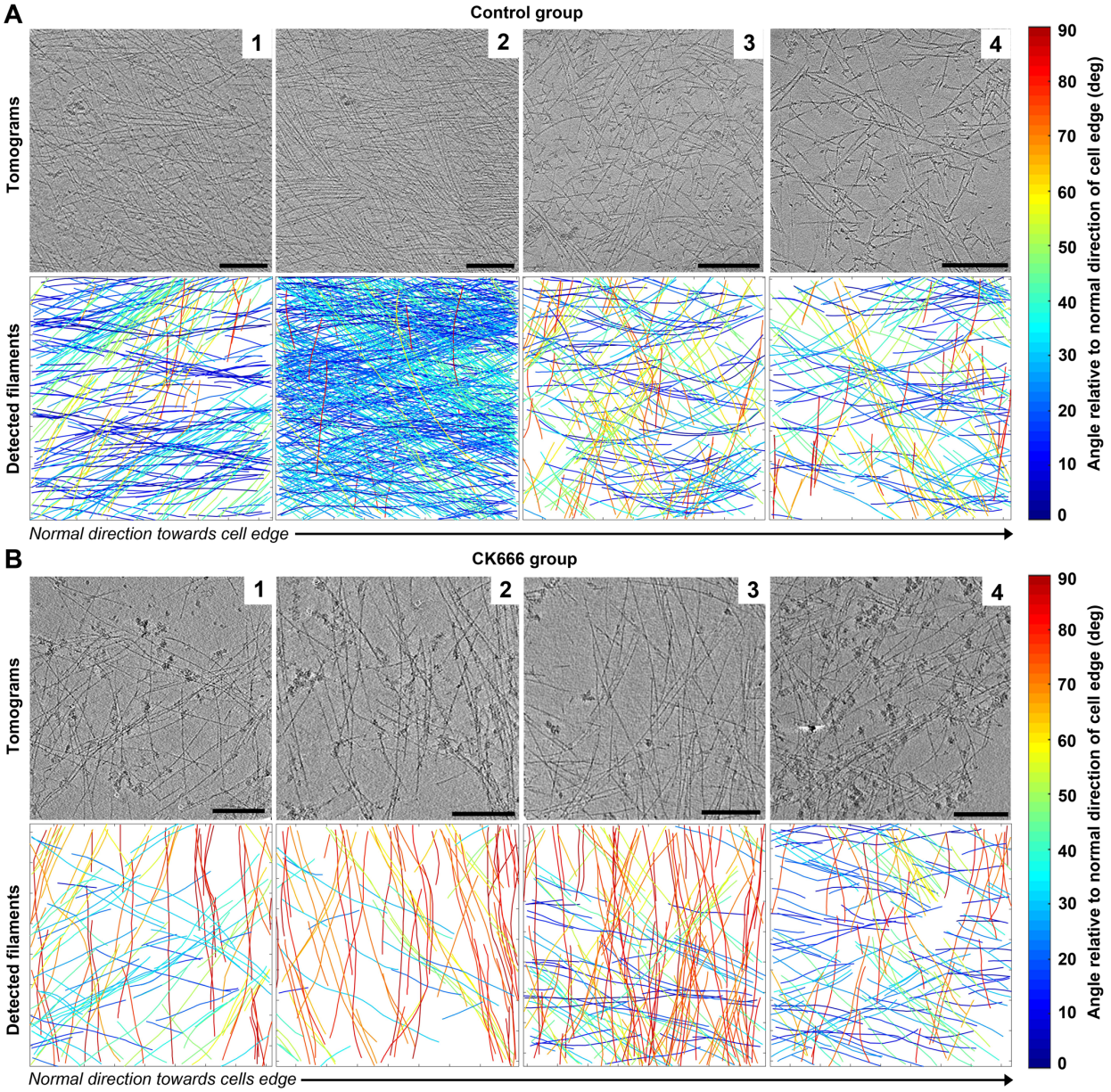

Suppl.Fig-4. Visual gallery of a lamellipodial dataset from extracted cells. A visual representation of all data files considered for quantitative analysis for **(A)** Lamellipodia of B16-F1 cells treated with DMSO (control) or **(B)** cells treated with Arp2/3 inhibitor CK666. Upper panels show 10 summed slices from representative bin8-tomograms. Bottom panels show computational toolbox-extracted visual output of analyzed coordinate files, color-coded for angular distribution of filaments to the cell edge. Black arrows indicate the orientation of the axis towards the cell edge in normal direction. All scale bars correspond to a length of 200nm. Note that the second panels (from left) for each group are also displayed in Figure-2.

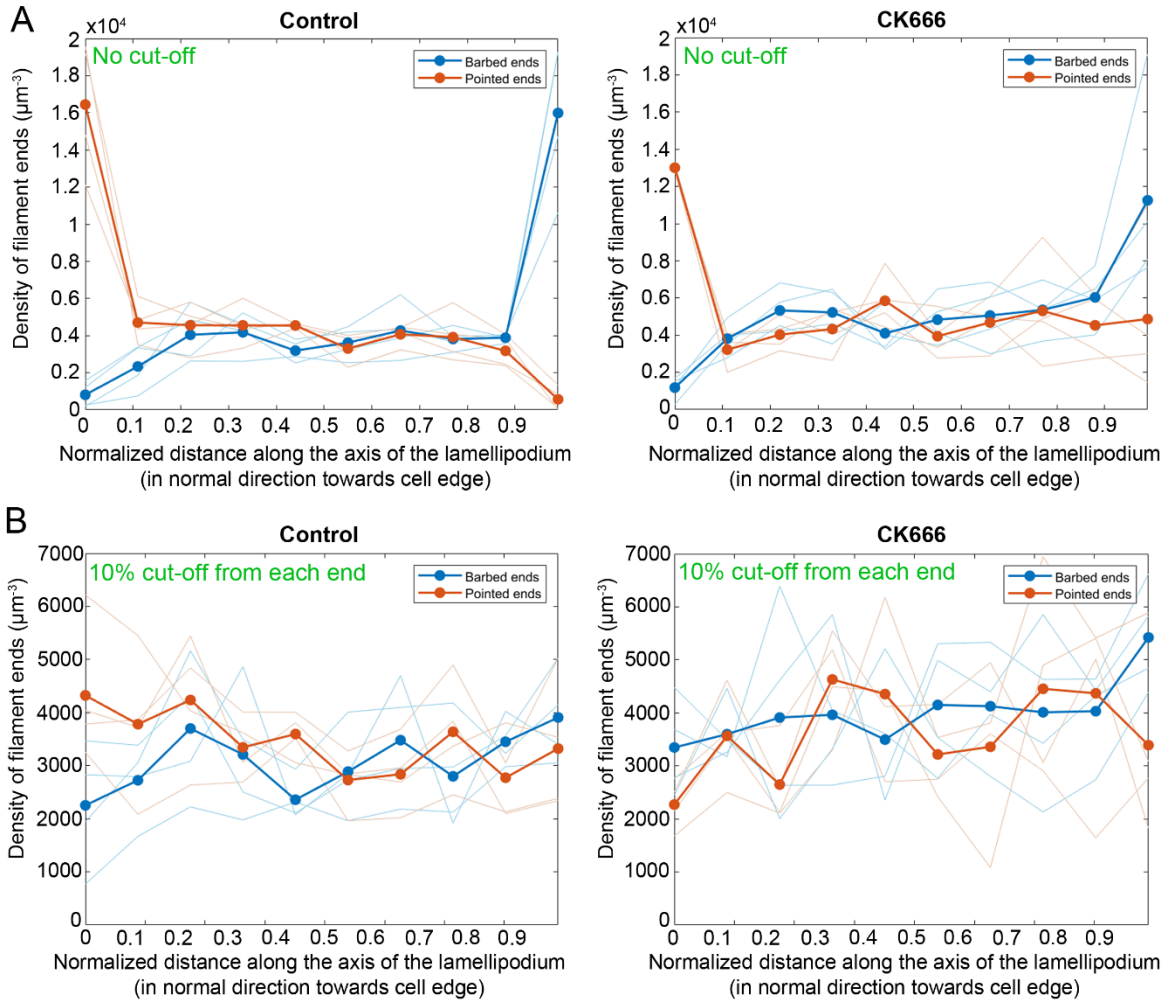

Suppl.Fig-5. Distribution of filament barbed and pointed ends along the lamellipodial axis. (A-B) The distribution of barbed and pointed ends of actin filaments is shown for B16-F1 cells treated with DMSO (as control, left panels) or with the Arp2/3 complex inhibitor CK666 (right panels). **(A)** No edge boundary cut-off was considered leading to an obvious accumulation of pointed and barbed ends at the back and front regions of the structure, respectively. **(B)** Same representation of the distribution of filament barbed and pointed ends along the axis of the lamellipodia, but excluding those positioned within the first and last 10% of the axis length. For all panels, thick lines indicate the values of barbed/pointed ends averaged for all data files in a group, while faint lines indicate the averaged values for individual data files.

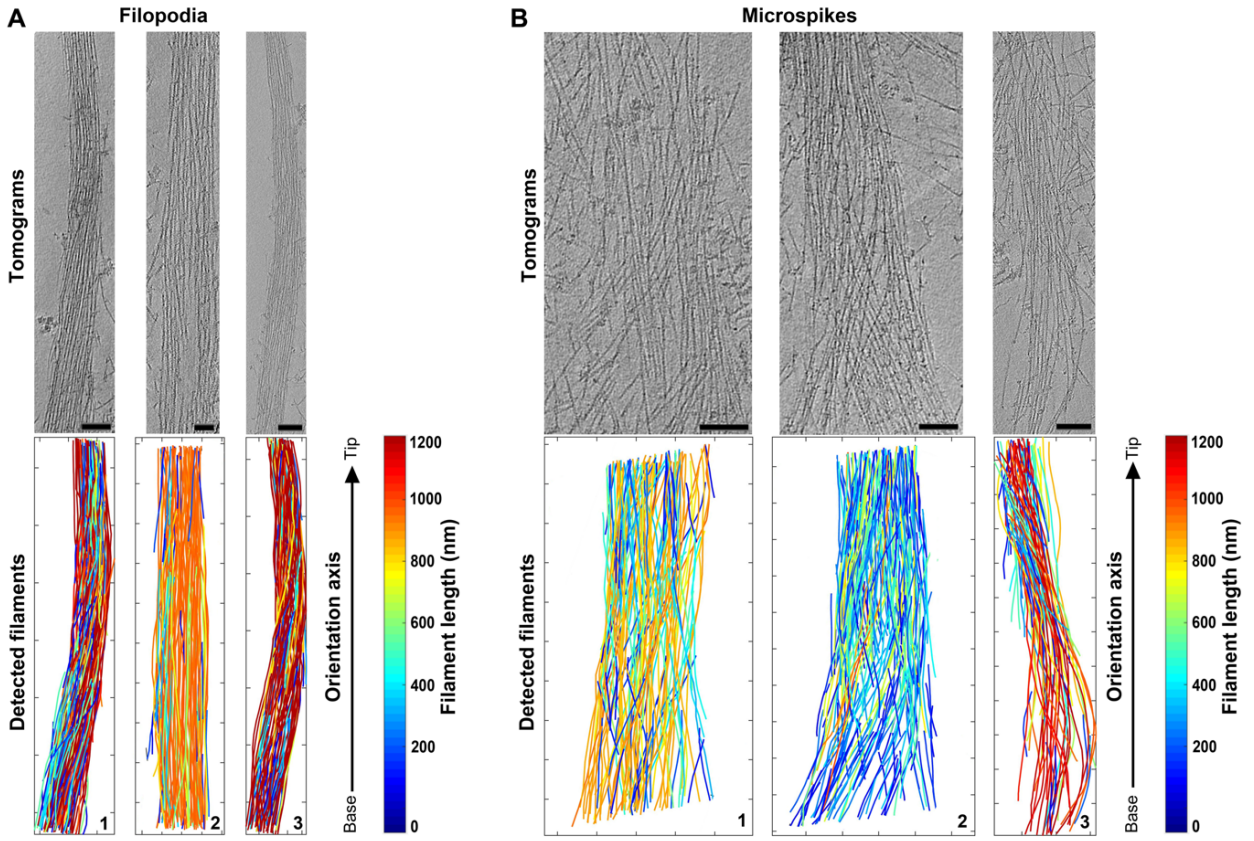

Suppl.Fig-6. Visual gallery of filopodia/microspikes dataset from extracted cells. A visual representation of all data files considered for quantitative analysis for **(A)** filopodia or **(B)** microspikes. Upper panels show 10 summed slices from representative bin8-tomograms, bottom panels show a typical visual output from the computational toolbox of analyzed coordinate files, color-coded for filament length. Black arrows indicate the direction of the axis towards the tip of the structure. All scale bars correspond to a length of 100nm. Note that the 3rd panels (numbers are indicated in the figure) for each group are also displayed in Figure-3.

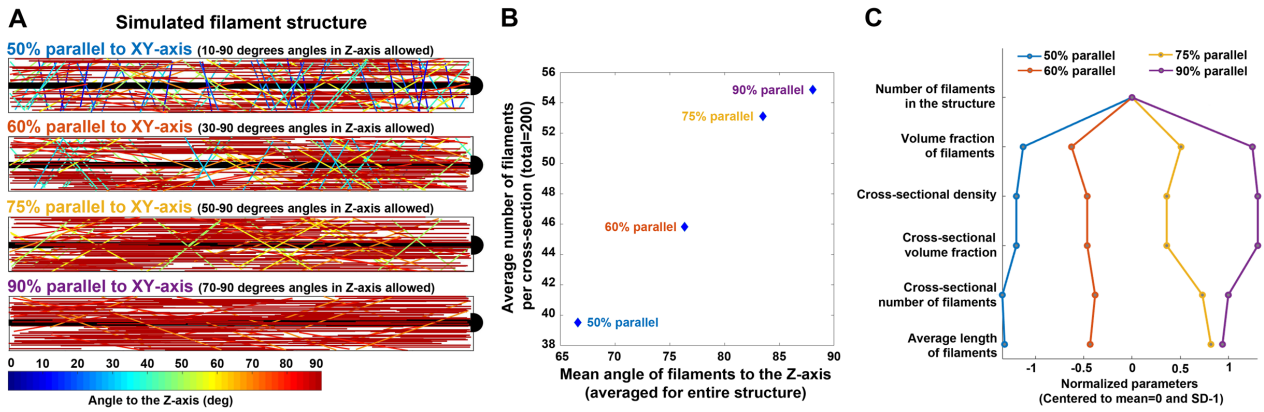

Suppl.Fig-7. Dependence of quantitative parameters on filament orientation to the Z-axis. (A) A series of filament structures (with a length of 400nm and height of 50nm) were simulated with a constant total number of 200 filaments, but with varying angular distribution of filaments in Z. From top to bottom, the degree of angular distribution and the total number of filaments running in acute angles to the XY-orientation axis were gradually reduced. **(B)** The data displayed in A was plotted in a 2D coordinate system to demonstrate that even in structures containing constant number of filaments, higher number of filaments running out of the XY plane results in a reduction of the average number of filaments per cross-section. **(C)** Angular distribution of filaments affects quantitative values of parameters describing cross-sectional characteristics.

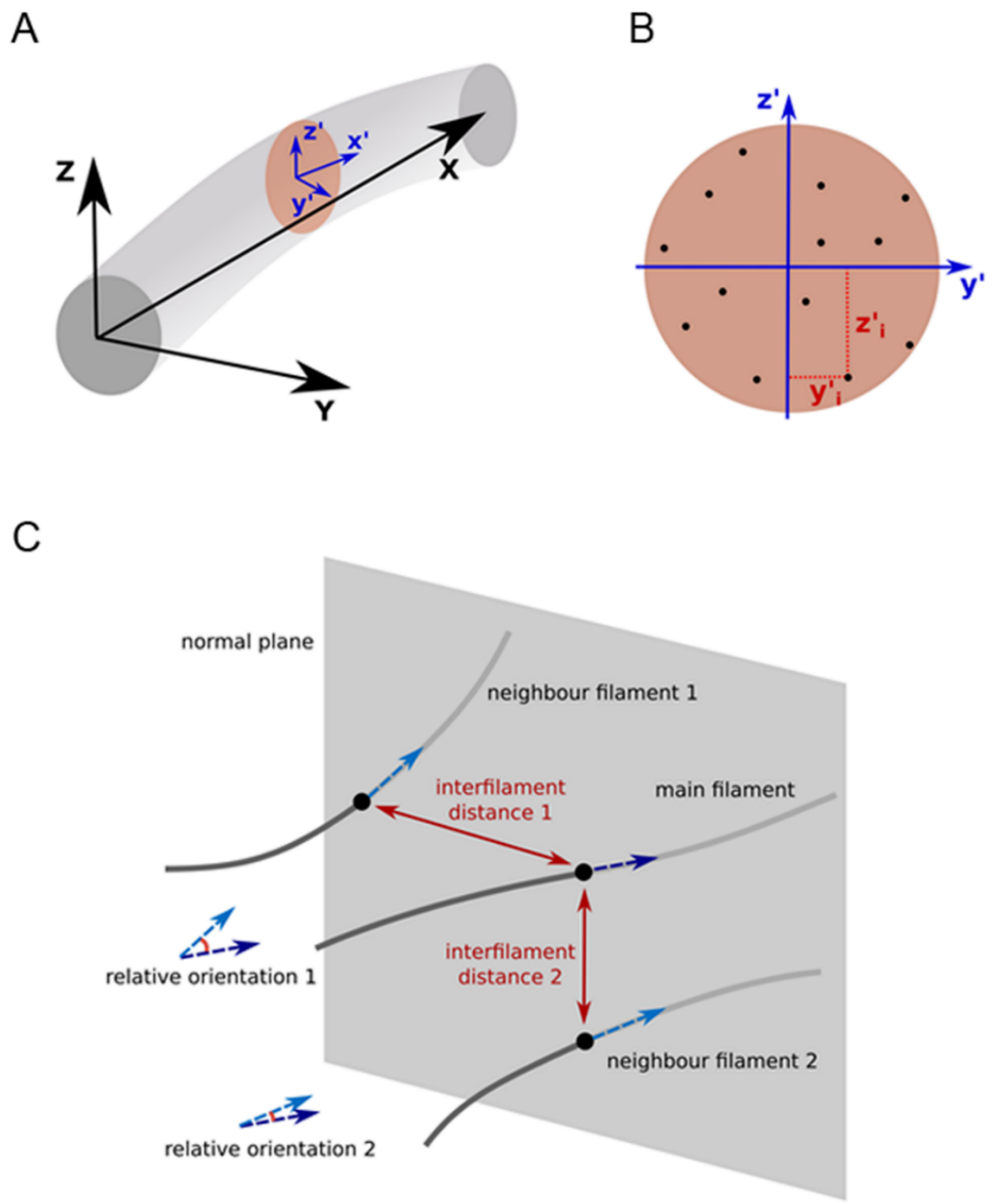

Suppl.Fig-8. Visual representation of geometry-based definitions used for deriving ultrastructural parameters. This figure graphically describes the parameters presented in the methods section. **(A)** The global frame of reference is shown with black letters and vectors. The local cross-sectional frame of reference is shown with blue letters and vectors for an arbitrary cross-section along the filopodium. **(B)** An example of defining the coordinates of a filament in the local cross-sectional frame of reference. Black dots indicate individual filaments intersecting with the cross section. **(C)** Inter-filament distances and relative orientations at a certain point on a filament with respect to two neighbor filaments. A normal plane is defined as a plane perpendicular to the main filament at an arbitrary point. Black dots show the intersections of filaments with the depicted normal plane. Dashed vectors are the tangent vectors of the filaments at the intersection points.

Supplementary References

Berg, S., Kutra, D., Kroeger, T., Straehle, C.N., Kausler, B.X., Haubold, C., Schiegg, M., Ales, J., Beier, T., Rudy, M., Eren, K., Cervantes, J.I., Xu, B., Beuttenmueller, F., Wolny, A., Zhang, C., Koethe, U., Hamprecht, F.A., Kreshuk, A., 2019. ilastik: interactive machine learning for (bio)image analysis. Nat. Methods 16, 1226–1232. https://doi.org/10.1038/s41592-019-0582-9

Winkler, C., Vinzenz, M., Small, J.V., Schmeiser, C., 2012. Actin filament tracking in electron tomograms of negatively stained lamellipodia using the localized radon transform. J Struct Biol 178, 19–28. https://doi.org/http://dx.doi.org/10.1016/j.jsb.2012.02.011